TRACKING WITH THE PEP-4 TPC*

A. Barbaro-Galtieri
Lawrence Berkeley Laboratory
University of California
Berkeley, CA 94720

Summary

The TPC has been tested with cosmic rays in July and November, 1981. It is now installed at IR2 at PEP and has been operating in 14 GeV e^+e^- beams for about a week. Preliminary analysis of the cosmic ray data yields spatial resolutions of $\sigma_{xy} = 260\ \mu$ and $\sigma_z = 650\ \mu$, at a pressure of 8.6 atm. Results are also reported at 4.0 and 1.5 atm. The operation with e^+e^- beams is good. No problems with positive ions feedback in the drift volume have been observed, so far. Events with up to 18 tracks have been reconstructed on line.

1.0 TPC

The Time Projection Chamber is a detector that provides 3-dimensional information on points along a track and, at the same time, provides information on energy loss that can be used for particle identification. A schematic drawing of the TPC used in the PEP-4 experiment[1] is shown in Fig. 1. It

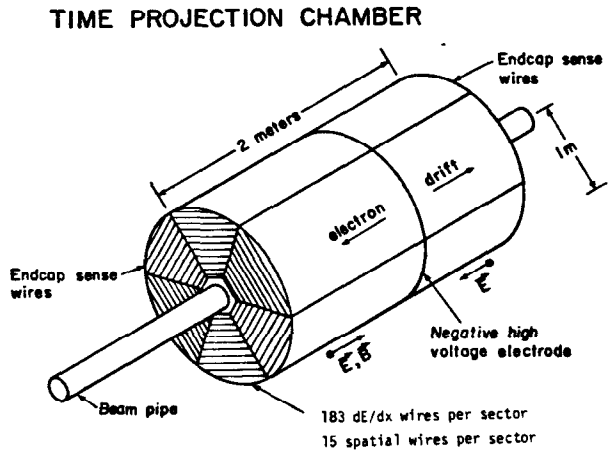

Fig. 1. A schematic drawing of the TPC.

is a 2 meter diameter, 2 meter long cylinder centered on the e^+e^- interaction region. The inner radius of the TPC is 20 cm, just sufficient to house a drift chamber, used for triggering purposes, and the beam pipe.

A particle traversing the cylinder volume will produce ionization along its path in the high pressure argon (80%)-methane (20%) mixture. The ionization electrons are drifted to the two endcaps by the electric field, parallel to the beam axis, provided by a central membrane kept at 75 KV negative potential at 8.6 atm gas pressure. A 4 KG magnetic field, parallel to the electric field, is produced by a conventional solenoidal coil. This coil will be replaced by a 15 KG superconducting coil in the future. In addition to providing sagitta information for the momentum measurement, the magnetic field is used to reduce the diffusion of the ionization electrons in the one meter drift to the endcap detectors.[2]

Each endcap consists of six proportional chambers (sectors). Each sector consists of a plane of grid wires (1 mm spacing), a plane of 183 sense wires (20 μ, 4 mm spacing) and field wires, and a ground plane. The total gap is 8 mm with the sense wire plane in the middle. The ground plane has 15 rows of pads etched in the copper, centered under 15 of the 183 sense wires. The pads are 7.5×7.5 mm squared and provide the x,y position measurements at 15 points along the track. The z coordinate is given by the time needed for the ionization to drift to the endcaps. The signal on the sense wires and pads is amplified and properly shaped[3] before going into charged coupled devices (CCD's) which provide pulse height measurements at 100 ns intervals (buckets). A signal is typically 5 buckets wide. The information of each bucket is digitized and then transferred to buffer memories. On each pad, clusters of neighboring buckets are then made to reconstruct the original signal and provide the z coordinate. The x position is obtained by finding the center of the pad clusters. The y position is given by the position of the pad row with some correction for oblique tracks. The TPC thus provides unambiguous 3-dimensional information. The expected resolution in x,y is 150 μ, in z is 350 μ. For tracking, the two track resolution is expected to be about 1 cm, both in xy and in z.

The sense wire pulse heights are used for measuring dE/dx, the energy loss by ionization, providing 183 samples for tracks at angles greater than 45^0 with the beam direction. For the time being the wires are not used for track reconstruction. For the 12 sectors a total of 2196 wire channels and 13848 pad channels are instrumented. Tracking with the TPC is discussed in this talk, dE/dx resolution is discussed in another contribution to this conference.[4]

2.0 Data

The data used for the resolution studies reported here were taken during the November 1981 test of the TPC. The TPC was placed inside the PEP-4 detector that included, besides the drift chamber around the beam pipe, a drift chamber outside the magnet coil and many layers of muon chambers interleaved with the iron of the return yoke. The cosmic rays used were required to have more than 0.6 GeV/c momentum. The two track segments were required to be in opposite sectors with respect to the beam line and to be collinear within 20 mr.

Data were taken at 8.6 atm, the operating pressure of the TPC, and also at 4.0 and 1.5 atm to study the pressure dependence of the resolution. Only 12 pad rows were instrumented for the test. Preliminary results[5] of the analysis of these data will be presented here.

*"This work was supported by the Director, Office of Energy Research, Office of High Energy and Nuclear Physics, Division of High Energy Physics of the U.S. Department of Energy under Contract No. DE-AC03-76SF00098."

3.0 Position Resolution

Only pad information is used for tracking, at this time. Important factors that determine the position resolution are: electronic noise, diffusion in the 1 m drift space, and ionization fluctuations. The geometry of the sectors and the electronics design were optimized to provide, for a given cost, a position resolution adequate to achieve a momentum resolution of $dp/p^2 = 0.4\%$ for a magnetic field of 15 KG. We will discuss below our understanding of the system at this time. More work is needed to achieve the desired resolution.

3.1 Pad Response

For the geometry of the TPC sectors the induced cathode signal on a pad receives contributions from the avalanches on the wire just above it and 2 more adjacent wires at each side. The couplings of the wires to the pads have been measured in a test set up with very similar geometry. The pad response has been found to have a shape very close to gaussian.[6] The σ_0 of the gaussian distribution for the present geometry is expected to be 3.5 mm, which means that a point on a track produces a signal in 3 pads or less. In order to achieve 150 μ resolution, the pulse height in the 3 pads will have to be measured with high precision, i.e., very low noise level and good electronic calibration is desirable. A discussion of the calibration of the system is included in ref. 4.

For the sample of events analysed, 12% of the points on tracks had signals on 3 pads, 79% had 2 pads, the remainder had 1 pad. For the 3-pad points we calculate the peak and the σ of the gaussian. For the 2-pad points we calculate the position of the peak using the σ information determined from the 3-pad data. The peak position provides the coordinate along the pad row. The y coordinate is determined by the center of the pad row. For tracks that traverse the pad row at an angle, correction to the y coordinate is obtained by using the pulse heights of the 5 wires contributing to the pad signals. This geometry, 5 wires contribute to one pad signal, has the advantage that the Landau ionization fluctuations are reduced in the pad signal.

We have parametrized the rms deviation of the gaussian pad response as follows:

$$\sigma^2 = \sigma_o^2 + \sigma_D^2 \, L/Lmax + \sigma_\alpha^2 \tan^2 \alpha \qquad (1)$$

where σ_0 depends only on the geometry of the sector, σ_D is the contribution due to diffusion and depends on the pressure of the TPC, L is the drift distance (L_{max} = 1 m), and σ_α includes the spreading of the gaussian response for tracks traversing the pads at an angle, α, defined in Fig. 2. The α dependence is due to broadening of the distributions when adding displaced gaussians for the 5 different wires and from Landau fluctuations within the collection region of each wire.

The α dependence is shown in Fig. 3 for the 8.6 atm data. We have not studied this effect in detail yet, the value obtained for the data in Fig. 3 is σ_α = 3.74 mm. The diffusion term is calculated from the dependence of σ on the drift length. This is shown in Fig. 4 for a run at 8.6 atm. Each data point corresponds to an average over many tracks at an average distance L from the sector. We have done some studies on the diffusion term and will discuss this in the next section.

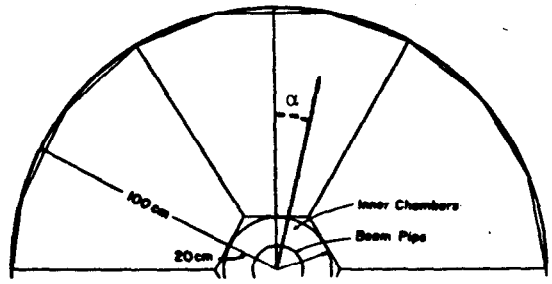

Fig. 2. Sector geometry. The angle α, local to each sector, is defined as the angle with the normal to the sector inner edge.

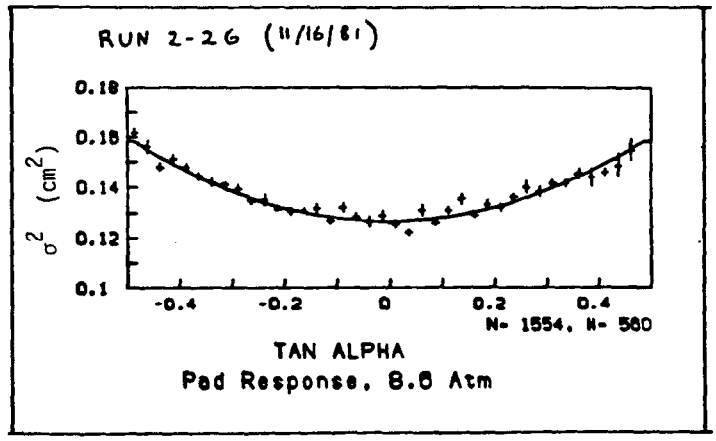

Fig. 3. Pad response dependence on α, for 8.6 atm data. The curve is a parabolic fit.

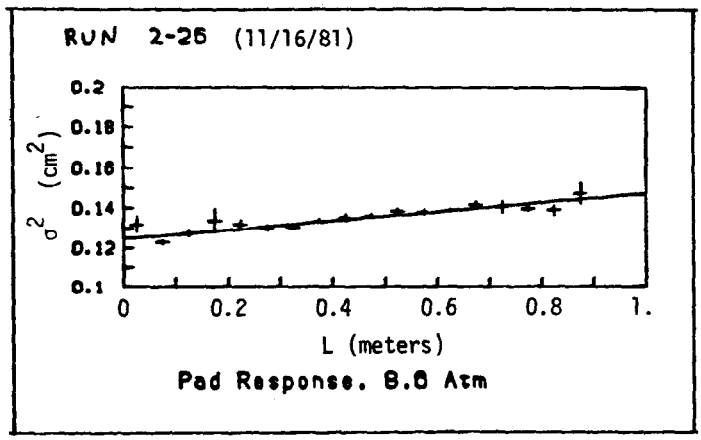

Fig. 4. Pad response dependence on L, drift distance, for 8.6 atm data. Average value over many tracks with the same L. A straight line fit is also shown.

When the data are corrected for the α and L dependence of formula (1), we get a distribution for σ_0 that looks gaussian as shown in Fig. 5. Table I shows the values of σ_0 obtained for different pressure and magnetic field conditions. As expected the measured σ_0 is independent upon these variables, indicating that all the data are internally consistent.

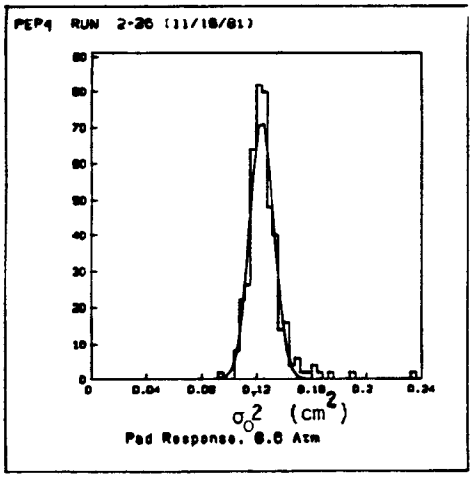

Fig. 5. Distribution of σ_o^2, the standard deviation of the gaussian pad response, after the L and α dependence have been corrected according to Eq. (1).

3.2 Diffusion

The diffusion dependence on the magnetic field, B, and on the pressure is shown in Table I. These values are averages over many runs, and the errors are statistical only. In absence of magnetic field the diffusion term increases with decreasing pressure with the $\sqrt{P}$ law, as expected. This can be seen in the values of σ_D for B = 0 shown in the last column, $\sigma_D \times \sqrt{P}$, which are scaled to 1 atm.

Table I. Pressure and B dependence of σ_0 and σ_D.

P (atm)	B (KG)	σ_0 (mm)	σ_D (mm)	$\sigma_D \times \sqrt{P}$ (mm)
8.6	0.	3.59 ± 0.04	1.44 ± 0.10	4.23 ± 0.41
4.0	0.	3.62 ± 0.03	2.05 ± 0.08	4.11 ± 0.15
1.5	0.	3.54 ± 0.05	3.30 ± 0.08	4.04 ± 0.10
8.6	3.9	3.59 ± 0.08	1.43 ± 0.05	4.20 ± 0.18
4.0	3.9	3.63 ± 0.02	1.71 ± 0.04	3.43 ± 0.05
1.5	3.9	3.51 ± 0.03	1.96 ± 0.06	2.40 ± 0.07

The comparison of the σ_D values for data with and without magnetic field is also of interest. We expect

$$\sigma_D(B) = \sigma_D(0)/\sqrt{1 + (\omega\tau)^2}$$

where $\omega = eB/cm$ and $\tau = 1.09 m v_d/eE$ are the cyclotron frequency of the electron and the mean collision time respectively, and v_d is the drift velocity. By taking the ratio of $\sigma_D(B)$ and $\sigma_D(0)$ we obtain measured values of $\omega\tau$, shown in Table II, and can compare them with the calculated values. Assuming $\omega\tau = 1.09\ v_d B/Ec$ and using the drift velocity measured in this experiment we calculate the values shown in Table II. The agreeement between $(\omega\tau)_m$ and $(\omega\tau)_c$ is quite good, again showing self consistency in the data that we are analyzing.

Table II. Drift velocity and $(\omega\tau)_m$ measured in this experiment. Values of $(\omega\tau)_c$ are shown for comparison.

P (atm)	E (KV/m)	$(\omega\tau)_m$	$(\omega\tau)_c$	v_d (cm/μsec)
8.5	75.0	0.10 ± 0.50	0.27	4.67 ± 0.08
4.0	35.0	0.66 ± 0.14	0.56	4.51 ± 0.09
1.5	13.2	1.36 ± 0.11	1.33	4.06 ± 0.08

The value of σ_D in Table I is the expected value for one electron. At different pressures we can estimate the effective number of electrons in the avalanche and calculate the contribution of diffusion to the resolution, as $\sigma_D/\sqrt{N}$. We obtain the values of 135 μ, 218 μ, and 404 μ for 8.6, 4.0, and 1.5 atm respectively, for 1 meter drift.

3.3 XY and Z Resolution

The spatial resolution is obtained by calculating the deviation of the pad points from the fitted track. The dependence of rmsxy on the drift distance L is shown in Fig. 6 for the 1.5 atm data.

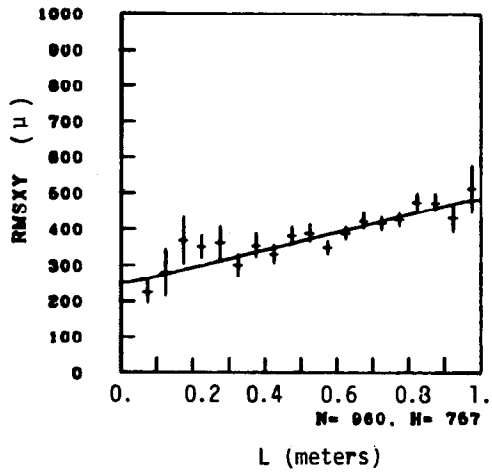

Fig. 6. Dependence of rmsxy on the drift distance for 1.5 atm data.

Here the effect of the diffusion is more pronounced than at higher pressure. The contribution of the diffusion can be calculated by taking the value of rmsxy at L = 1.0 m and subtracting in quadrature from it the value at L = 0. We find:

$$(\text{rmsxy})_D = 420 \pm 23\ \mu$$

which is in good agreement with the value of 404 μ calculated in the previous section from the pad response.

The dependence of rmsxy on α for one of the runs at 8.6 atm is shown in Fig. 7. Although the statistics is not large, it is evident that there is an α dependence for $|\alpha| > 15^o$. It is independent of angle for $|\alpha| < 10^o$ and we can use this region to calculate the actual σ_{xy}. The distribution of rmsxy for these events is shown in Fig. 8 for the 8.6 atm data. To calculate the resolution we take

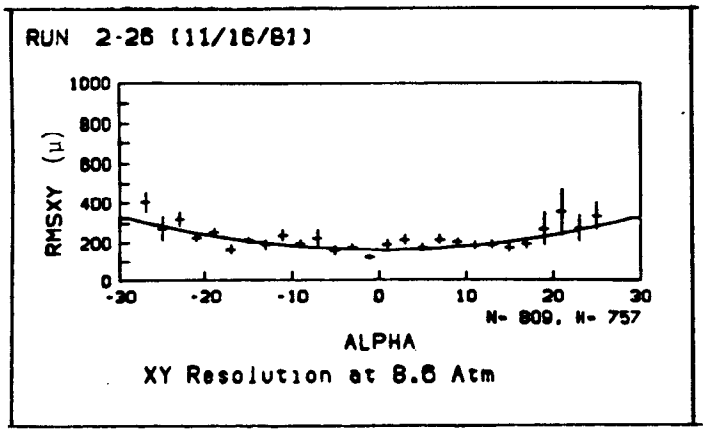

Fig. 7. Dependence of rmsxy on the angle α for 8.6 atm data.

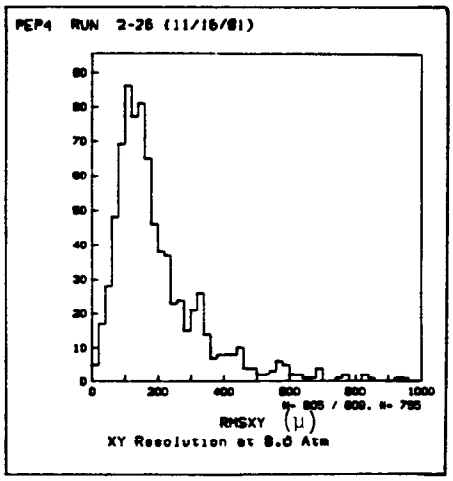

Fig. 8. Distribution of rmsxy for tracks with $|\alpha| < 10^{\circ}$. From it we obtain $\sigma_{xy} = 260\ \mu$.

the mean of this distribution and add it in quadrature to its standard deviation. Note that the distribution of Fig. 8 is not gaussian and that the peak value falls well below the quoted resolution. At the different pressures we obtain the values shown in Table III.

We use a similar method to measure the z resolution. We see little dependence of rmsz on L, the drift distance, therefore we average over all tracks. The distribution of rmsz has a similar behavior as Fig. 8, and the average is calculated in the same way as for σ_{xy}. The results are shown in Table III.

Table III. Resolution in xy and z at different pressures.

P(atm)	$\sigma_{xy}(\mu)$	$\sigma_z(\mu)$
8.6	260	654
4.0	299	810
1.5	439	857

The xy resolution of 8.6 atm is worse than the 150 μ we expected to achieve. There are many factors that can deteriorate the resolution.

(a) Electronic noise. The noise level at this time is about 2.4 counts, i.e., 1% of the signal for a minimum ionizing track. This is expected to contribute 64 μ to the resolution.

(b) The electronic calibration is not optimized. We are working on improving the stability of the system.

(c) We expect distortions due to $E \times B$ effects, that is effects due to radial components of B. We have not included these corrections in the analysis yet. Corrections are expected to be as large as 120 μ.

(d) Electrostatic distortions. The electric field is not uniform across the drift volume. We have observed some distortions in regions very close to the inner and outer radius of the TPC. Corrections for these distortions are not included.

The z resolution is also worse than expected, but again electronic noise and unreliable calibration affect this resolution.

We expect to improve the resolution when these effects are better understood and corrected.

4.0 Momentum Resolution

This can be calculated by comparing the curvature of the cosmic rays in the two track sections in opposite sectors. The distribution of the difference of curvatures for one of the data runs at 8.6 atm is shown in Fig. 9. The rms

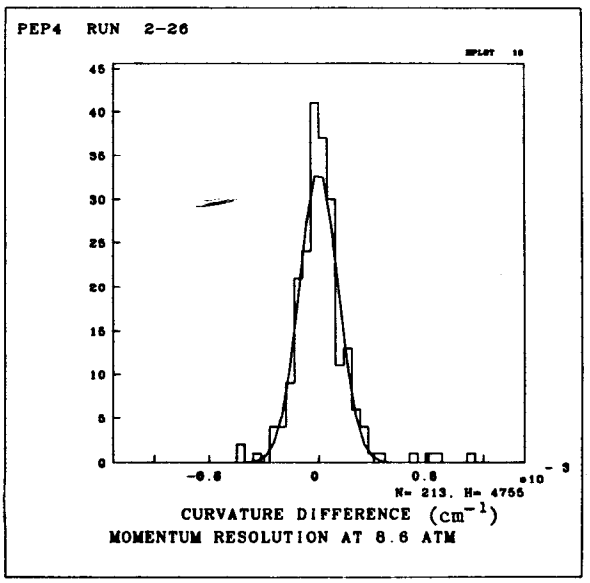

Fig. 9. Distribution of curvature difference for the same cosmic ray in two track portions. The standard deviation of this distribution yields $dp/p^2 = 0.081(\text{GeV/c})^{-1}$.

deviation of this distribution, after normalization, gives $dp/p^2 = 0.081\ (\text{GeV/c})^{-1}$. The resolution we expect to achieve for a 4 KG field is $dp/p^2 = 0.016\ (\text{GeV/c})^{-1}$.

At this time the measured resolution is a factor 5.1 worse than expected. Part of this discrepancy is due to the electrostatic distortions we mentioned earlier. For this reason, a shorter track length is used in the fit; two inner and two outer pad rows are not included. We are presently studying the time stability of the distortions and how to correct for them.

The dp/p^2 resolution depends on the point resolution, σ_{xy}, the length of the track measured, L, the magnetic field, and the number of measured points, N, approximately according to the relation:

$$dp/p^2 \propto \sigma_{xy}/(BL^2\sqrt{N})$$

For a 4 KG field, this dependence would predict a deterioration of the resolution by a factor 4.5; we observe a factor 5.1. This indicates that the momentum resolution we measure is not inconsistent with the results discussed so far. By correcting for the known effects we expect to improve the resolution considerably.

5.0 Performance of the TPC in e+ e- Beams

The TPC has been operating for a week at PEP in 14 GeV beams. An event with 16 prongs reconstructed on line is shown in Fig. 10 and 11.

Figure 10 shows the projection of the event on the endcaps. Only pad clusters were used for track reconstruction. Each track found is identified by a number or a letter. The algorithm used was developed on Monte Carlo data; improvements are needed. Most clusters not associated with tracks are due to electronics noise.

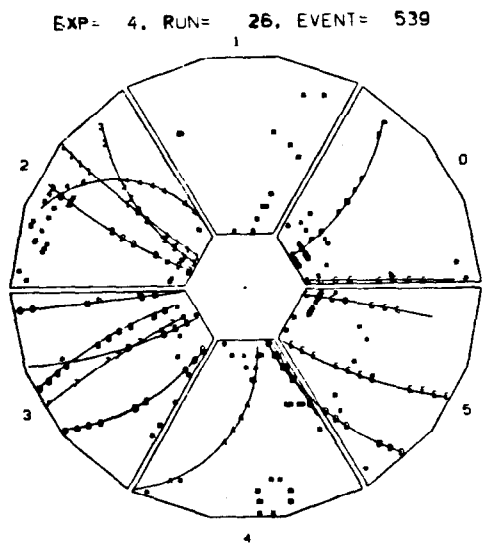

Fig. 10. End view of an hadronic event observed in 14 GeV e^+e^- beams. The event was reconstructed on line using only pad data.

Figure 11 shows the wire information for the tracks, found using pad data, in one of the sectors; specifically tracks one through 4. The peculiar band with no data is due to a group of 16 electronics channels missing at the time the event was detected. Bad z calibration can be seen here by noticing that groups of 16 channels are out of line. There are some unassociated clusters. One set is clearly a spiraling electron. Another set, in the upper corner, is due to the tail of a saturated pulse, not properly shaped. This problem is now understood and being fixed.

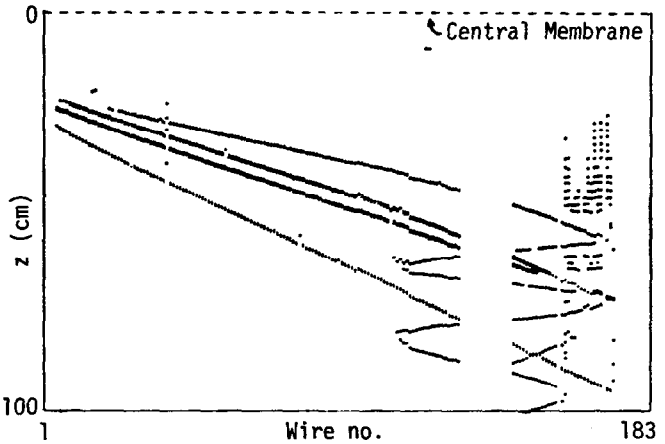

Fig. 11. Wire information in one of the sectors for 4 tracks of the event of Fig. 10.

So far, we have not detected any large effects due to positive ion feedback. More detailed analysis is needed. The luminosity during data taking was 5×10^{30} cm^{-2}/sec or less.

References

1. Proposal for a PEP Facility based on the Time Projection Chamber, Johns Hopkins University, Lawrence Berkeley Laboratory, University of California at Los Angeles, University of California at Riverside, Yale University; PEP Experiment No. 4, SLAC report PUB-5012 (1976).

2. D. R. Nygren, The Time Projection Chamber, SLAC and LBL Reports PEP-144 (1974), and PEP-198 (1975). D. Fancher et al., Nucl. Inst. and Meth. 161, 383 (1979).

3. R. C. Jared, D. A. Landis, and F. S. Goulding, IEEE Trans. on Nucl. Science, Vol. NS-29 (1982) and LBL Report LBL-13183 (1981).

4. G. R. Lynch and N. J. Hadley, Energy Loss Measurements in the PEP TPC. These Proceedings.

5. L. Galtieri, N. Hadley, and G. Lynch, "Preliminary Results of the November TPC Test," LBL Report LBL-TPC-82-01 (1982).

6. A. C. Schaffer and D. L. Fancher, LBL Report TPC-LBL-77-44 (1977).